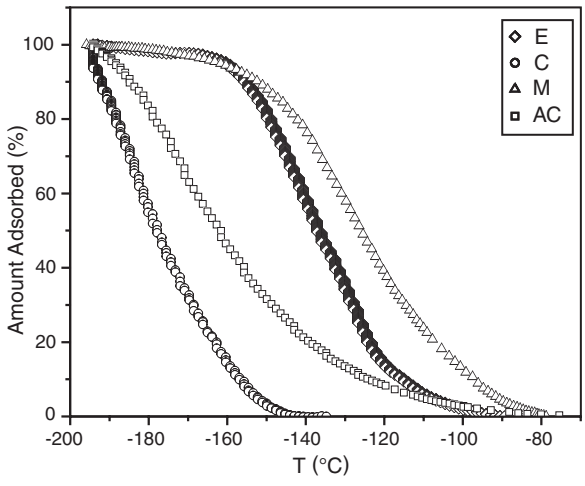

Fig. 4. Isobars for hydrogen desorption from adsorbents **AC** (squares), **E** (diamonds), **M** (triangles), and **C** (circles) at 1 bar hydrogen pressure.

at low temperature compared with **C**, attributed to adsorption in the ultrananoporosity (<0.5 nm). The isosteric enthalpy for H_2 adsorption on **AC** at zero surface coverage is low, at 4.03(7) kJ mol^{-1} (temperature range –196°C to –159°C) (figs. S5 to S6) (*21*). This result is entirely consistent with desorption isobar characteristics of H_2 from **AC** decreasing rapidly with increasing temperature.

Porous structures **E** and **M** have quite different isobar *T* dependence compared with **AC** and **C**. The lack of desorption of H_2 up to about –160°C is consistent with the isotherm hysteresis shown in Fig. 2. Desorption from **E** and **M** is thus kinetically limited at low *T*. As *T* is increased, thermal motion allows desorption of the trapped H_2 guest to occur via window opening, which becomes noticeable at –160°C, with complete desorption at about –80°C. The narrow window systems thus outperform the larger pore materials **AC** and **C** at higher temperatures because of kinetic trapping of H_2.

Hydrogen adsorption on widely different porous structures is very sensitive to *T*, consistent with thermodynamics for H_2 adsorption on activated carbon [enthalpy of adsorption ~4 kJ mol^{-1} (figs. S3 to S6)], driving desorption well below room temperature. Given the intrinsic difficulty in tuning the carbon surface–H_2 van der Waals interaction to compete with thermal energies, the development of carbon-based adsorbents for H_2 storage is extremely challenging. There is an intrinsic conflict between the large pore volume required to enhance H_2 storage capacity and the resulting decrease in the strength of the interaction in wider pores. The hysteresis in H_2 uptake in porous MOF materials, where the pore window dimensions are similar to the kinetic diameter of H_2, differs qualitatively from more rigid classical sorbents. Hydrogen can be loaded under high *P* and stored at low *P* if the cavities are larger than the windows (Fig. 1D), which in turn are both close in size to H_2 and have sufficient flexibility due to framework dynamics to allow kinetic trapping of the guest. The current materials are still certainly not practical storage materials with respect to U.S. Department of Energy guidelines (6 weight percent being a target for 2010, versus ~1.0 for our best material). However, the design of porous MOF materials to include thermally activated windows in the open channel structure offers the possibility of modifying their desorption kinetics to improve their hydrogen storage characteristics.

References and Notes

1. "Grand challenge for basic and applied research on hydrogen storage: statement of objectives," available at www.eere.energy.gov/hydrogenandfuelcells/docs/gc_h2_storage.doc.
2. G. Gundiah, A. Govindaraj, N. Rajalakshmi, K. S. Dhathathreyan, C. N. R. Rao, *J. Mater. Sci.* **85**, 209 (2003).
3. A. J. Fletcher, K. M. Thomas, *Langmuir* **16**, 6253 (2000).
4. C. R. Reid, K. M. Thomas, *J. Phys. Chem. B* **105**, 10619 (2001).
5. J. L. C. Rowsell, A. R. Millward, K. S. Park, O. M. Yaghi, *J. Am. Chem. Soc.* **126**, 5666 (2004).
6. G. Ferey *et al.*, *Chem. Commun.* **2003**, 2976 (2003).
7. D. N. Dybtsev, H. Chun, S.-H. Yoon, D. Kim, K. Kim, *J. Am. Chem. Soc.* **126**, 32 (2004).
8. L. Pan *et al.*, *J. Am. Chem. Soc.* **126**, 1308 (2004).
9. O. M. Yaghi, H. Li, C. Davis, D. Richardson, T. L. Groy, *Acc. Chem. Res.* **31**, 474 (1998).
10. R. Kitaura, K. Seki, G. Akiyama, S. Kitagawa, *Angew. Chem. Int. Ed. Engl.* **42**, 428 (2003).
11. M. Eddaoudi *et al.*, *Acc. Chem. Res.* **34**, 319 (2001).
12. S. L. James, *Chem. Soc. Rev.* **32**, 276 (2003).
13. K. Endo *et al.*, *J. Am. Chem. Soc.* **119**, 4117 (1997).
14. M. Kondo, T. Yoshitomi, K. Seki, H. Matsuzaka, S. Kitagawa, *Angew. Chem. Int. Ed. Engl.* **36**, 1725 (1997).
15. P. Losier, M. J. Zaworotko, *Angew. Chem. Int. Ed. Engl.* **35**, 2779 (1996).
16. K. N. Power, T. L. Hennigar, M. J. Zaworotko, *New J. Chem.* **22**, 177 (1998).
17. C. J. Kepert, M. J. Rosseinsky, *Chem. Commun.* **1999**, 375 (1999).
18. A. J. Fletcher, E. J. Cussen, C. J. Kepert, M. J. Rosseinsky, K. M. Thomas, *J. Am. Chem. Soc.* **123**, 10001 (2001).
19. E. J. Cussen, J. B. Claridge, M. J. Rosseinsky, C. J. Kepert, *J. Am. Chem. Soc.* **124**, 9574 (2002).
20. D. Bradshaw, T. J. Prior, E. J. Cussen, J. B. Claridge, M. J. Rosseinsky, *J. Am. Chem. Soc.* **126**, 6106 (2004).
21. Materials and methods are available as supporting material on *Science* Online.
22. K. S. W. Sing *et al.*, *Pure Appl. Chem.* **57**, 603 (1985).
23. A. J. Fletcher, E. J. Cussen, D. Bradshaw, M. J. Rosseinsky, K. M. Thomas, *J. Am. Chem. Soc.* **126**, 9750 (2004).
24. This work was partly supported by the Carbon Trust, the Engineering and Physical Sciences Research Council, and the Northwest Molecular Materials Centre. X-ray coordinates have been deposited with the Cambridge Crystallographic Data Centre (M.2CH_3OH: 248270; E.2C_2H_5OH: 114887; C.3$C_3H_6(OH)_2$: 225153; and C: 225154).

Supporting Online Text

www.sciencemag.org/cgi/content/full/1101982/DC1
Materials and Methods
Tables S1 and S2
Figs. S1 to S9

25 June 2004; accepted 4 October 2004
Published online 14 October 2004;
10.1126/science.1101982
Include this information when citing this paper.

Long-Term Aridity Changes in the Western United States

Edward R. Cook,[1]* Connie A. Woodhouse,[2] C. Mark Eakin,[2] David M. Meko,[3] David W. Stahle[4]

The western United States is experiencing a severe multiyear drought that is unprecedented in some hydroclimatic records. Using gridded drought reconstructions that cover most of the western United States over the past 1200 years, we show that this drought pales in comparison to an earlier period of elevated aridity and epic drought in AD 900 to 1300, an interval broadly consistent with the Medieval Warm Period. If elevated aridity in the western United States is a natural response to climate warming, then any trend toward warmer temperatures in the future could lead to a serious long-term increase in aridity over western North America.

More than 50% of the coterminous United States experienced moderate to severe drought conditions in 2002, with record or near-record precipitation deficits throughout the western United States (*1*). Large portions of the Canadian Prairie provinces also suf-

fered from severe drought, as well as extensive areas of Mexico, particularly in the northern and western parts of the country. In many of these areas, the 2002 drought was actually part of an ongoing drought that started in late 1999 or before, with widespread drought conditions already persisting for ~3 years. Drought abated in many areas by late 2002 to early 2003, but severe drought conditions have continued to affect the interior western United States throughout the 2004 summer (*2*).

This drought highlights both the extreme vulnerability of the semi-arid western United States to precipitation deficits and the need to better understand long-term drought variability and its causes in North America. To this end, we have used centuries-long, annually resolved tree-ring records to reconstruct annual changes in both drought and wetness over large portions of North America. The reconstructed drought metric is the summer-season Palmer Drought Severity Index (PDSI) (*3*), a widely used measure of relative drought and wetness over the United States (*4*) and other global land areas (*5*, *6*).

New PDSI reconstructions have been produced on a 286-point 2.5° by 2.5° regular grid (Fig. 1) (*7*). This grid covers most of North America and is a substantial expansion of an earlier 155-point 2° by 3° drought reconstruction grid that covered only the coterminous United States (*8*). In addition, our drought reconstructions are 600 to 1200 years long over much of the U.S. portion of the North American grid (particularly in the western United States), a substantial increase over the ~300 years available from the previously published reconstructions, which all began in 1700. Finally, the variance restoration we apply to the grid point reconstructions (*7*) allows for updates of those records to AD 2003 with instrumental PDSI data. Together, these attributes enable us to compare the current western U.S. drought to those that are reconstructed to have occurred as far back as AD 800, a time period that includes the so-called Medieval Warm Period (MWP).

The region of interest here is contained within an irregular black polygon on the North American grid (Fig. 1), an area that we henceforth refer to simply as the West. Each of the 103 grid points in the West has a summer PDSI reconstruction that covers the common interval AD 1380 to 1978, with a minimum of 68 grid points having reconstructions that extend back to AD 800. These reconstructions were produced with a well-tested principal components regression procedure developed previously to robustly reconstruct drought across the coterminous United States (*8*, *9*), but now with a much denser network of 602 centuries- to millennia-long tree-ring chronologies used as predictors of PDSI (*7*). As before (*8*), a split calibration and verification scheme was used to

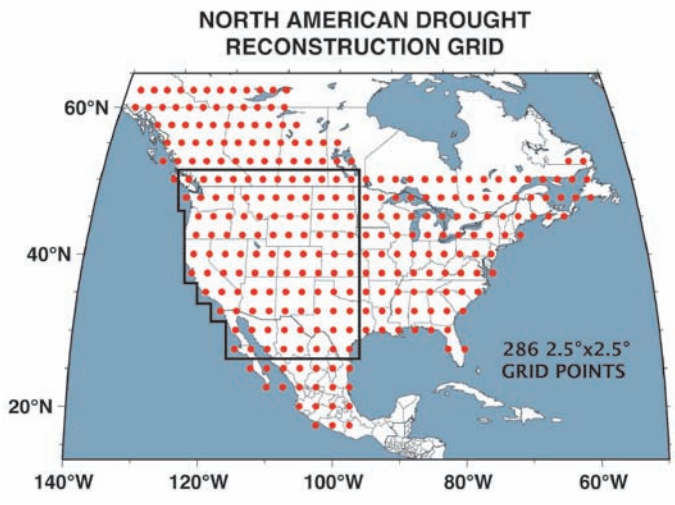

Fig. 1. The North American summer drought reconstruction grid and the (mostly) western U.S. region, circumscribed by the thick black irregular polygon. Out of the 286 total grid points, 103 are contained within the Western region. Each of the 103 grid points has an annually resolved drought reconstruction that extends back to at least AD 1380, with 68 extending back to AD 800. These form the basis for our reconstruction of area affected by drought in the West (*7*).

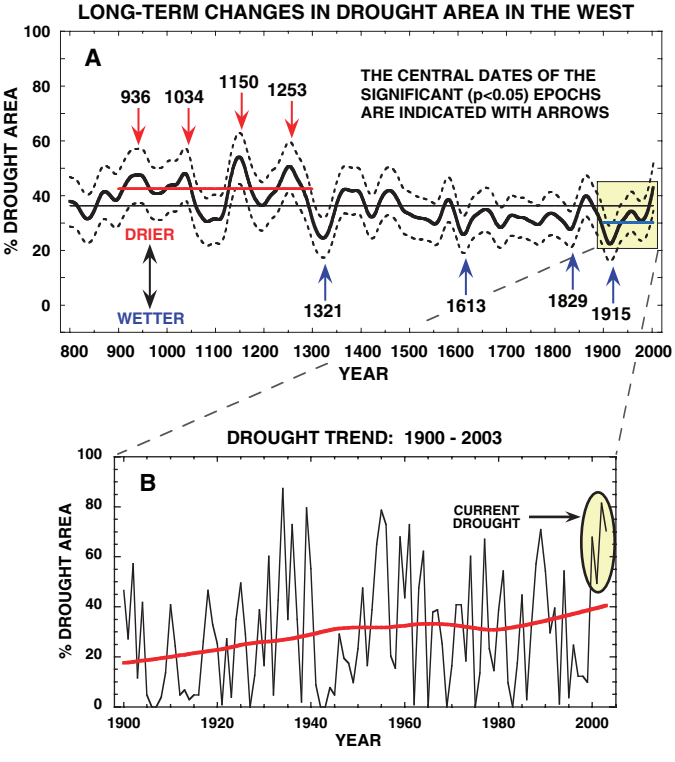

Fig. 2. (**A**) Smoothed DAI reconstruction (solid black curve) for the West, showing two-tailed 95% bootstrap confidence intervals (dashed black curves) and the long-term mean (thin horizontal black line). Sixty-year smoothing was applied to highlight the multidecadal to centennial changes in aridity. The four driest epochs ($P < 0.05$, those with confidence limits above the long-term mean in Fig. 2A) are before AD 1300, whereas the four wettest ($P < 0.05$) epochs occur after that date. The difference between the means of the AD 900 to 1300 period (red line, 42.4%) and AD 1900 to 2003 period (blue line, 30%) are also apparent. The 12.4% difference between the two periods translates into an average drought area (PDSI < –1) increase of 41.3% in the West during the earlier period. This difference is statistically significant ($P < 0.001$) given an equality-of-means *t* test with degrees of freedom corrected for first-order autocorrelation. Even so, some of the AD 900 to 1300 period PDSI estimates are extrapolations, because they fall outside the range of the instrumental PDSI data in the AD 1928 to 1978 calibration period (*7*). As regression-based estimates, these extrapolations have greater uncertainty compared to those that fall within the range of the calibration period. However, they are still based on the actual growth histories of highly drought-sensitive trees. Therefore, we argue that our DAI reconstruction is indicative of what really happened in the West, even during the AD 900 to 1300 period of elevated aridity (*7*). (**B**) The annually resolved AD 1900 to 2003 portion, which more clearly reveals the severity of the current drought relative to others in the 20th century and an irregular trend (red smoothed curve) toward increasing aridity since 1900.

[1]Lamont-Doherty Earth Observatory, Palisades, NY 10964, USA. [2]National Oceanic and Atmospheric Administration (NOAA), National Climatic Data Center, Boulder, CO 80305, USA. [3]Laboratory of Tree-Ring Research, University of Arizona, Tucson, AZ 85721, USA. [4]Department of Geosciences, University of Arkansas, Fayetteville, AR 72701, USA.

*To whom correspondence should be addressed. E-mail: drdendro@ldeo.columbia.edu

develop and test the grid point regression models, with time-varying subsets of tree-ring predictors used this time at each grid point to maximize the lengths of the PDSI reconstructions (*7*) (fig. S1). Tests of the time-varying subset approach (*7*) (fig. S3) indicate that this method produces reconstructions with highly significant hindcast skill, especially when the reconstructions are examined as a Western regional average (*10*).

At this spatial scale, it is possible to critically examine the long-term history of drought in the West over the past 1200 years. For this purpose, we used the Drought Area Index (DAI) (*7*). The DAI is a simple count of the number of grid point reconstructions that exceed a given threshold of PDSI (e.g., PDSI < -1) in any given year, with the number of grid points exceeding the threshold divided by the total number of grid points to provide an estimate of percent area affected by drought. As such, it is a nonparametric expression of the area affected by drought over a given domain. Because any grid point can potentially contribute to the total area affected by drought, the DAI also implicitly absorbs the natural spatial variability of the expressed PDSI patterns from year to year.

Before calculating the Western DAI reconstruction, we restored the lost variance due to regression in each time-varying subset grid point PDSI reconstruction to that of the instrumental data (*7*). Doing so corrected for temporal and spatial variations in explained PDSI variance (i.e., the regression coefficient R^2) over the drought grid, which provided DAI estimates based on the full amplitude of reconstructed PDSI variability. Restoring the lost variance had no meaningful effect on the relative changes in aridity presented here (*7*). Consequently, variance restoration mainly operates here as a bias correction that increases the DAI to that which is presumably closer to what really happened in the past.

After restoring the lost variance to the PDSI reconstructions, we updated them from 1979 to 2003 with appended, gridded instrumental data (*7*) (fig. S4). This allowed the current drought to be put in its proper long-term perspective. We also conducted a "frozen grid" analysis of the DAI to determine if the decline in available grid points from 103 in AD 1380 to 68 in AD 800 (*7*) (figs. S2 and S5) might have a negative effect on the fidelity of the DAI reconstruction. The loss of spatial information in the Western DAI record before AD 1380 was found to be negligible.

The Western DAI reconstruction (Fig. 2A) is based on a PDSI < -1 threshold with 2-tailed 95% bootstrap confidence limits (*7*). The annual DAI estimates have been smoothed with a 60-year low-pass filter to highlight multidecadal or longer changes in drought area. Doing so emphasizes some earlier increases in aridity that dwarf the comparatively short-duration current drought in the West. Expressing the DAI reconstruction in this filtered way does not minimize the effect of the current multiyear drought (Fig. 2B). Rather, it emphasizes the fact that more intense droughts of longer duration have occurred in the past and could occur in the future. The four driest epochs ($P < 0.05$), centered on AD 936, 1034, 1150, and 1253, all occurred during a ~400-year interval of overall elevated aridity from AD 900 to 1300. This time period is broadly consistent with the MWP, an epoch noted for both anomalous warmth (*11*) and hydroclimatic variability (*12*) in parts of the West. The DAI reconstruction also reveals an abrupt change to persistently less arid conditions after AD 1300 (*13*, *14*) that lasted for ~600 years, up to about AD 1920. The four lowest aridity epochs ($P < 0.05$), which culminate with the early 20th century "pluvial" (*15*), are found during this post–AD 1300 interval.

Since the turn of the 20th century, overall aridity in the West has increased in an irregular manner. The high-resolution segment of the reconstruction (Fig. 2B) shows the classic Dust Bowl drought of the 1930s and the severe 1950s' drought. Although the current drought does not differ greatly from those past episodes in terms of maximum annual percent area affected, its 4-year duration appears to be unusual over the past 104 years. Compared to the earlier "megadroughts" that are reconstructed to have occurred around AD 936, 1034, 1150, and 1253, however, the current drought does not stand out as an extreme event, because it has not yet lasted nearly as long. This finding shows that the West can experience far more severe droughts than any found in the 20th century instrumental climate record, including the current one.

With this in mind, it is important to validate the occurrence of our AD 900 to 1300 elevated aridity period. There are numerous independent indicators of past aridity that have been described from various subregions in the West. These indicators include in situ tree stumps in lakebeds and river channels (in California) (*12*), an above-average frequency of fire scars on trees (in California) (*16*), elevated charcoal in lake sediments (in California, Idaho, and Wyoming) (*17*–*19*), increased lake salinity (in North Dakota) (*20*), sand dune activation (in Nebraska) (*21*), changes in lake sediment oxygen isotope ratios (in Nevada) (*22*), and lichen oxalate residue (in Texas) (*23*). Although these records vary in dating accuracy and resolution, they provide independent direct or inferred evidence of elevated aridity in the AD 900 to 1300 period (Fig. 3), which collectively supports the more temporally and spatially complete DAI evi-

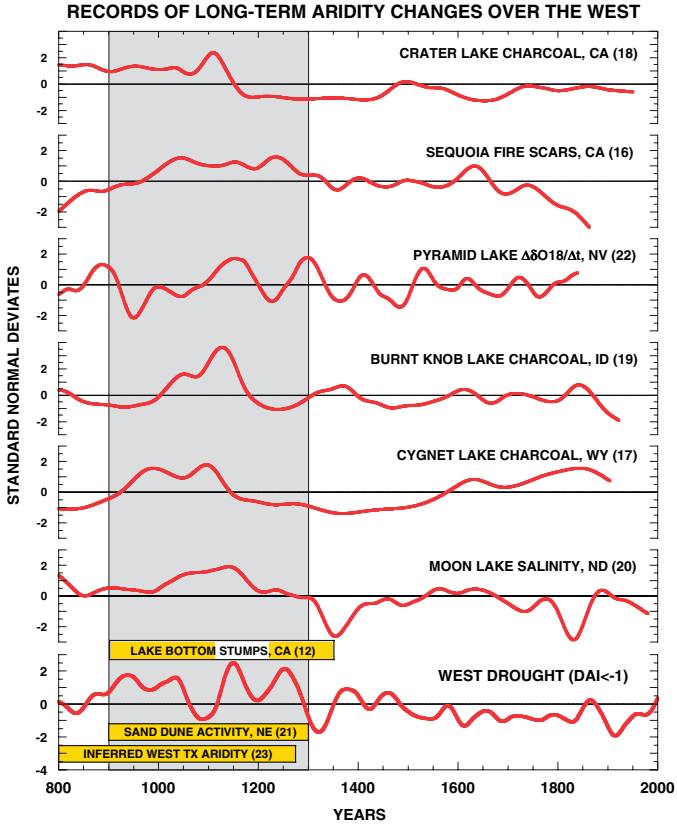

Fig. 3. Nine independent records of long-term aridity changes in subregions of the West (*12*, *16*–*23*) compared to the DAI reconstruction. All of the time series records have been smoothed to highlight multidecadal to centennial variations and are expressed as standard normal deviates for comparison purposes. The yellow bars are dated intervals of aridity. The break in the yellow bar for the "lake bottom stumps" indicates two dry periods separated by a wetter interval. The shaded tan area highlights the period of persistently elevated aridity in the DAI record over the AD 900 to 1300 period. These independent records all show multidecadal intervals of elevated aridity during that time, which collectively support our DAI reconstruction based on long, drought-sensitive, tree-ring records. Numbers in parentheses are citations.

dence for our 400-year epoch of unprecedented drought severity and duration in the West.

Given this result and the effect of the current drought on the West, it is critically important to understand how the AD 900 to 1300 megadrought epoch could have developed and persisted for so long. In so doing, it might be possible to determine the likelihood that we could return to a similar time of more intense and prolonged aridity. The overall coincidence between our megadrought epoch and the MWP suggests that anomalously warm climate conditions during that time may have contributed to the development of more frequent and persistent droughts in the West. Coupled ocean-atmosphere model runs with elevated atmospheric greenhouse gases also suggest that anomalous surface warming over interior North America will lead to increased summer dryness from elevated evapotranspiration demand and reduced soil moisture content (*24*).

Pacific Ocean variability also modulates moisture transport into the West on interannual to multidecadal time scales (*25*). These teleconnected influences on drought and wetness have been linked to a variety of climate modes, including the El Niño–Southern Oscillation (ENSO) and Pacific decadal variability (e.g., the Pacific Decadal Oscillation) (*26–28*), which can act together to enhance drought development in the West. Decadal variability in the Atlantic Ocean has also been associated with large-scale U.S. droughts (*28*), but no causal mechanism for this has yet been presented, particularly west of the Great Plains. There is also evidence for a 20th-century trend in U.S. drought frequency being associated with increasing Northern Hemisphere temperatures (*28*), with anomalous late 20th-century warming of western Pacific and Indian Ocean sea surface temperatures (SSTs) also contributing since 1998 to the development of droughts over mid-latitude areas of the Northern Hemisphere (*29*). Thus, large-scale warming, such as what plausibly occurred during the MWP, is again suggested as a contributor to the AD 900 to 1300 epoch of elevated aridity and epic drought in the West.

Anomalous warming over the tropical Pacific Ocean may also lead to increased drought frequency in the West through the way that it promotes enhanced upwelling in the eastern Pacific "cold tongue" region. This Bjerknes-style dynamical response of the coupled ocean-atmosphere system to exogenous heating of the tropical atmosphere has been argued on both observational and theoretical grounds (*30*). The resulting enhanced upwelling promotes the development of La Niña–like, cool SSTs over the eastern tropical Pacific, a condition that is associated with drought in the West (*26*).

Additional support for this mechanism of drought development in the West has recently emerged by radiatively forcing the Zebiak-Cane (Z-C) ENSO model with changing volcanic forcing and solar irradiance over the past 1000 years (*31*). The volcanic signal consists of a series of impulsive radiative forcing events from explosive eruptions in equatorial regions, that affect tropical Pacific SSTs on the relatively short El Niño–La Niña time scale. In contrast, lower frequency solar forcing results in a weaker, more equilibrated, SST response on multidecadal and longer time scales.

When the Z-C model is forced in this way, eastern tropical Pacific SSTs tend toward a cool, La Niña–like base state during the model run's early period (circa AD 1100 to 1250) of high solar irradiance and reduced volcanism. This result is supported by evidence of extreme drought in Peru during medieval times (AD 800 to 1250) (*32*), an interval that is very similar to our AD 800 to 1300 epoch of elevated aridity. Thus, the Z-C model results (*31*) provide a plausible physical mechanism for how protracted La Niña–like conditions could have developed during the MWP, a drought-inducing condition for both Peru (*32*) and the West (*26*).

If the Z-C modeling results hold up, it is plausible that continued warming over the tropical Pacific, whether natural or anthropogenically forced, will promote the development of persistent drought-inducing La Niña–like conditions. Should this situation occur, especially in tandem with midcontinental drying over North America, the epoch of unprecedented aridity revealed in the DAI reconstruction might truly be a harbinger of things to come in the West.

References and Notes

1. J. Lawrimore, S. Stephens, "Climate of 2002 annual review" (NOAA National Climatic Data Center, available at http://lwf.ncdc.noaa.gov/oa/climate/research/2002/ann/events.html), 2003.
2. D. Miskus, *U.S. Drought Monitor* (National Centers for Environmental Prediction/National Weather Service/NOAA, Climate Prediction Center, available at www.drought.unl.edu/dm/monitor.html), 2004.
3. W. C. Palmer, "Meteorological drought" (Res. Pap. No. 45, U.S. Department of Commerce Weather Bureau, Washington, DC, 1965).
4. R. R. Heim Jr., *Bull. Am. Meteorol. Soc.* **83**, 1149 (2002).
5. A. Dai, K. E. Trenberth, T. R. Karl, *Geophys. Res. Lett.*, **25**, 3367 (1998).
6. A. Dai, K. E. Trenberth, T. Qian, *J. Hydrometeorol.*, in press.
7. Materials and methods are available as supporting material on *Science* Online.
8. E. R. Cook, D. M. Meko, D. W. Stahle, M. K. Cleaveland, *J. Clim.* **12**, 1145 (1999).
9. Z. Zhang, M. E. Mann, E. R. Cook, *Holocene* **14**, 502 (2004).
10. The calibration and verification statistics used to assess the goodness-of-fit and validity of the PDSI reconstructions are (i) the calibration period coefficient of multiple determination or regression R^2 (CRSQ), (ii) the verification period square of the Pearson correlation coefficient or r^2 (VRSQ), (iii) the reduction of error (RE), and (iv) the coefficient of efficiency (CE) (*8*). The magnitudes of these statistics, as measures of explained variance, are strongly dependent on the number of tree-ring chronologies available for PDSI reconstruction at each grid point (*7*) (fig. S3). When these statistics are calculated for the 103–grid point West regional average PDSI reconstruction, CRSQ, VRSQ, RE, and CE are 0.86, 0.73, 0.78, and 0.72, respectively, for the most highly replicated post-1800 period of the reconstruction, based on a median of 41 tree-ring predictors per grid point reconstruction, and 0.68, 0.54, 0.64, and 0.53, respectively, when based on the smallest subset of tree-ring predictors available at the start of each grid point reconstruction (a median of 2 per grid point) (*7*) (fig. S3). Although there is indeed a decline in calibration and verification skill as the number of tree-ring chronologies available for reconstruction declines, the latter set of statistics still indicates highly significant hindcast skill.
11. V. C. LaMarche Jr., *Science* **183**, 1043 (1974).
12. S. Stine, *Nature* **369**, 546 (1994).
13. Other high-resolution paleoclimate records from lakes scattered across the northern prairies of North America also show abrupt moisture regime shifts around the AD 1300 period.
14. K. R. Laird *et al.*, *Proc. Natl. Acad. Sci. U.S.A.* **100**, 2483 (2003).
15. F. K. Fye, D. W. Stahle, E. R. Cook, *Bull. Am. Metereol. Soc.* **84**, 901 (2003).
16. T. W. Swetnam, *Science* **262**, 885 (1993).
17. S. H. Millspaugh, C. Whitlock, P. J. Bartlein, *Geology* **28**, 211 (2000).
18. J. A. Mohr, C. Whitlock, C. N. Skinner, *Holocene* **10**, 587 (2000).
19. A. Brunelle, C. Whitlock, *Quat. Res.* **60**, 307 (2003).
20. K. R. Laird, S. C. Fritz, K. A. Maasch, B. F. Cumming, *Nature* **384**, 552 (1996).
21. J. A. Mason, J. B. Swinehart, R. J. Goble, D. B. Loope, *Holocene* **14**, 209 (2004).
22. L. Benson *et al.*, *Quat. Sci. Rev.* **21**, 659 (2002).
23. J. Russ, D. H. Loyd, T. W. Boutton, *Quat. Int.* **67**, 29 (2000).
24. R. T. Wetherald, S. Manabe, *Clim. Change* **43**, 495 (1999).
25. A. Gershunov, T. P. Barnett, *Bull. Am. Meteorol. Soc.* **79**, 2715 (1998).
26. J. E. Cole, J. T. Overpeck, E. R. Cook, *Geophys. Res. Lett.* **29**, 10.1029/2001GL013561 (2002).
27. M. Barlow, S. Nigam, E. H. Berbery, *J. Clim.* **14**, 2105 (2001).
28. G. J. McCabe, M. A. Palecki, J. L. Betancourt, *Proc. Natl. Acad. Sci. U.S.A.* **101**, 4136 (2004).
29. M. Hoerling, A. Kumar, *Science* **299**, 691 (2003).
30. M. A. Cane *et al.*, *Science* **275**, 957 (1997).
31. M. E. Mann, M. A. Cane, S. E. Zebiak, A. Clement, *J. Clim.*, in press.
32. B. Rein, A. Lückge, F. Sirocko, *Geophys. Res. Lett.* **31**, L17211, 10.1029/2004GL020161 (2004).

33. We gratefully acknowledge the NOAA International Tree-Ring Data Bank (www.ncdc.noaa.gov/paleo/treering.html) and its many contributors for much of the tree-ring data used in this work. In addition, many tree-ring records not yet in the public domain were kindly contributed to our drought reconstruction project by a number of tree-ring scientists doing work in the United States, Canada, and Mexico. All are gratefully appreciated. We also thank M. A. Cane, R. Seager, M. E. Mann, and two anonymous reviewers for helpful comments. Drought reconstructions discussed in this paper can be found at www.ncdc.noaa.gov/paleo/pdsi.html. Supported by NOAA grant no. NA06GP0450 and NSF grant no. ATM 03-22403. This is Lamont-Doherty Earth Observatory contribution no. 6681.

Supporting Online Material

www.sciencemag.org/cgi/content/full/1102586/DC1
SOM Text
Figs. S1 to S5
References and Notes

9 July 2004; accepted 17 September 2004
Published online 7 October 2004;
10.1126/science.1102586
Include this information when citing this paper.